JACS
JOURNAL OF THE AMERICAN CHEMICAL SOCIETY

Article

pubs.acs.org/JACS

Fluorescence Quenching Studies of Potential-Dependent DNA Reorientation Dynamics at Glassy Carbon Electrode Surfaces

Qin Li, Chenchen Cui, Daniel A. Higgins,* and Jun Li*

Department of Chemistry, Kansas State University, Manhattan, Kansas 66506, United States

Supporting Information

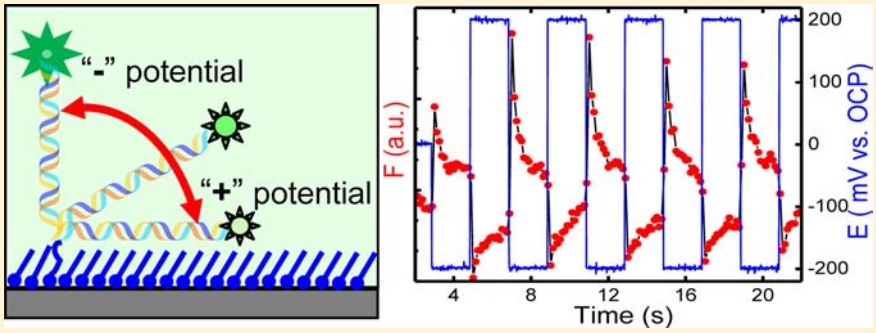

ABSTRACT: The potential-dependent reorientation dynamics of double-stranded DNA (ds-DNA) attached to planar glassy carbon electrode (GCE) surfaces were investigated. The orientation state of surface-bound ds-DNA was followed by monitoring the fluorescence from a 6-carboxyfluorescein (FAM6) fluorophore covalently linked to the distal end of the DNA. Positive potentials (i.e., +0.2 V vs open circuit potential, OCP) caused the ds-DNA to align parallel to the electrode surface, resulting in strong dipole−electrode quenching of FAM6 fluorescence. Switching of the GCE potential to negative values (i.e., −0.2 V vs OCP) caused the ds-DNA to reorient perpendicular to the electrode surface, with a concomitant increase in FAM6 fluorescence. In addition to the very fast (submilliseconds) dynamics of the initial reorientation process, slow (0.1−0.9 s) relaxation of FAM6 fluorescence to intermediate levels was also observed after potential switching. These dynamics have not been previously described in the literature. They are too slow to be explained by double layer charging, and chronoamperometry data showed no evidence of such effects. Both the amplitude and rate of the dynamics were found to depend upon buffer concentration, and ds-DNA length, demonstrating a dependence on the double layer field. The dynamics are concluded to arise from previously undetected complexities in the mechanism of potential-dependent ds-DNA reorientation. The possible origins of these dynamics are discussed. A better understanding of these dynamics will lead to improved models for potential-dependent ds-DNA reorientation at electrode surfaces and will facilitate the development of advanced electrochemical devices for detection of target DNAs.

INTRODUCTION

The development of fast, sensitive, inexpensive, and portable DNA sensors that can be integrated into miniaturized biochips is critical for point-of-care diagnosis and in-field screening. Such sensors are based on the detection of specific DNA targets through their hybridization with complementary single stranded (ss) oligonucleotide probes immobilized at the surface of a sensing device.[1] While a number of optical methods have been used for DNA sensing, electrochemical methods offer unique advantages that may afford improved speed and specificity.[1,2] For example, while the working electrode in an electrochemical device serves to transform DNA hybridization events into electrical signals, it can also be used to generate an electric field to actively manipulate the hybridization process. Indeed, it has already been demonstrated that a positive electropotential can be used to concentrate DNA targets at an electrode surface and accelerate hybridization, while a negative electropotential can be used to enhance discrimination between matched and mismatched sequences.[3−5]

Recently, Rant, et al. have employed fluorescence quenching methods to explore the potential-dependent dynamics of dye-labeled DNA on Au surfaces.[6−8] They discovered that surface-bound double stranded (ds) DNA molecules behaved as rigid rods that could be readily reoriented by the strong field of the electrical double layer (EDL). DNA orientation was affected even when only a fraction of its length was exposed to the field and when the potential was modulated at frequencies up to several kHz. In these experiments, reorientation of the ds-DNA at negative and positive electrode potentials caused the fluorescent dye attached at its distal end to extend away from or fold onto the electrode surface, respectively, resulting in an increase or decrease in the fluorescence signal. Quenching of the fluorescence in such experiments occurs by dipole−electrode energy transfer,[6−8] when the dye is in close proximity to the electrode surface. In contrast, ss-DNA showed greatly

Received: May 9, 2012
Published: August 10, 2012

   dx.doi.org/10.1021/ja304512k | J. Am. Chem. Soc. 2012, 134, 14467−14475

reduced fluorescence modulation, due to its greater flexibility. The differences between ss- and ds-DNA dynamics were shown to provide a unique method for detecting DNA hybridization.[6,7]

While the work highlighted above demonstrates the significant promise of these methods for advanced DNA detection, the mechanisms by which DNA molecules interact with the strong EDL fields at an electrode surface are complex and not yet fully understood. It is well-known that the electropotential quickly drops to insignificant levels over distances of ∼1 nm in normal physiological buffers (i.e., 1× phosphate-buffered saline, PBS). Hybridized ds-DNA molecules in biosensors are relatively long in comparison (e.g., ds-DNA consisting of 20 base pairs is ∼7 nm in length), meaning that only a short segment of the DNA is actually exposed to the EDL field. If the buffer is diluted 100 fold, the EDL thickness is increased to ∼10 nm and becomes comparable to the ds-DNA length, but the field strength is also reduced at the same potential. Complex dynamics are also expected as the EDL charges and discharges following a change in the electrode potential. These dynamics are further complicated by the participation of the negatively charged phosphate-sugar backbone of the DNA in EDL charging/discharging. Notably, the bound charges on the DNA are expected to respond differently to a change in potential than do the free ions of the buffer. As a result, the charge distribution within the EDL at a DNA-functionalized electrode may be very different from that predicted by Gouy−Chapman−Stern theory[9] both immediately after a change in the electrode potential and under steady-state conditions.

In this paper, we report new investigations into the mechanisms of potential-dependent DNA dynamics at glassy carbon electrode (GCE) surfaces. Carbon electrodes offer several potential advantages over metals;[10] these include lower cost, wider potential window (see Figure S1 [Supporting Information (SI)]), improved chemical stability, high electrocatalytic activity, and flexible chemistry for robust covalent functionalization. GCEs also represent an important model system upon which future studies of emerging carbon nanofiber materials can be based.[11] Two oligonucleotide probes of different lengths (34 bases and 45 bases) were covalently attached to the GCE surface for the present studies. The oligonucleotides were labeled at the distal end with a 6-carboxyfluorescein (FAM6) fluorophore. FAM6 fluorescence was strongly quenched in close proximity to the electrode surface but quickly increased when moved away. Modulation of FAM6 fluorescence reflects the potential-dependent reversible reorientation of the negatively charged DNA molecules within the EDL. In addition to the fast dynamics (instrument limited, subms time scale) of ds-DNA switching originally observed by Rant et al.,[6] the present results also depict a new, slower relaxation process (>0.1 s time scale). The fluorescence profiles obtained from the reorientation dynamics experiments were quantitatively explained by nonradiative energy transfer between the dye and GCE surface, assuming a dye−surface distance (d) dependence proportional to $1/d^4$.[12,13] The amplitudes of both the fast and slow components as well as the rate of the slow component were found to strongly depend upon salt concentration for 0.2×, 0.067×, 0.02×, and 0.0067× PBS buffers. Furthermore, longer ds-DNA molecules (45 bases) showed larger-amplitude fluorescence modulation and faster relaxation than the shorter ones (34 bases). The results suggest that the negatively charged DNA molecules may be actively involved in EDL reconstruction following a change in the electropotential.

EXPERIMENTAL SECTION

DNA Molecules. DNA oligonucleotides were purchased from the Midland Certified Reagent Co. Included were oligonucleotide probes of 34 bases (34-mer, P1) and 45 bases (45-mer, P2), and their complementary targets T1 and T2. Their sequences are listed below:

P1: FAM6-5′-AAGAAGAAGACAGCAAAGAGCAAGT-CTTCTTCTT-3′-Dabcyl-dT-aminoC7
T1: 5′-AAGAAGAAGACTTGCTCTTTGCTGTCTT-CTTCTT-3′
P2: FAM6-5′-AAGAAGAAGAAGAAGCAGCAAAGAG-CAAGCCTTCTTCTTCTTCTT-3′-Dabcyl-dT-aminoC7
T2: 5′-AAGAAGAAGAAGAAGGCTTGCTCTTTGCTG-CTTCTTCTTCTTCTT-3′.

The length of the hybridized probe−target pairs was estimated to be 11.22 nm for 34-mer and 14.85 nm for 45-mer ds-DNA, respectively using an Internet tool.[14] AminoC7 represents a standard linker $-H_2C-CH(CH_2OH)-CH_2-CH_2-CH_2-CH_2-NH_2$ incorporated by the oligonucleotide vendor, which provided a primary amine group at the end for covalent attachment to the GCE surface and a flexible alkane chain to reduce steric effects at the surface.

Glassy Carbon Electrode Preconditioning. Glassy carbon plates of 17 mm × 15 mm × 2 mm (SPi supplies) were used as electrodes. The GCEs were freshly polished with 0.05 μm γ alumina slurry on napless polishing cloth (Buehler) for 5 min, followed by washing and sonicating in deionized water for 15 min. The electrodes were then electrochemically activated by etching in 1.0 M NaOH by cycling the electrode potential between −0.1 and 1.2 V (vs saturated calomel electrode, SCE) in one cycle, at a scan rate of 50 mV/s. This procedure was found to provide the most reproducible GCE surface with abundant carboxylic acid groups available for DNA attachment.

DNA Functionalization and Hybridization. The DNA probes were covalently attached to the GCE surface by formation of an amide bond between the amine group on the 3′ end of each DNA molecule and a carboxylic acid group on the GCE surface. In this procedure, the GCE was incubated in 50 μL of 1.0 μM DNA in 1× PBS solution (137 mM NaCl, 2.7 mM KCl, 8.1 mM $Na_2HPO_4{\cdot}H_2O$, and 1.76 mM KH_2PO_4) at 40 °C for 1 h, in the presence of 1-ethyl-3-[3-dimethylaminopropyl]carbodiimide hydrochloride (25 mM) and *N*-hydroxysulfosuccinimide (10 mM) catalysts. After rinsing, the remaining −COOH groups on the functionalized electrodes were passivated by reaction with 1.0 mM hexylamine solution containing the same catalysts. Hybridization to the surface-bound DNA was accomplished by incubating the probe/hexylamine-modified GCEs in 5.0 μM complementary target in 2× saline sodium citrate (SSC) buffer (0.30 M NaCl and 30 mM trisodium citrate) at 75 °C for 1 h and then slowly cooling to room temperature. Over 70% of the ss-DNA probes were found to form ds-DNA, as measured by chronocoulometry. The modified GCEs were rinsed and stored in pH = 7.0 20× SSC buffer at 4 °C prior to use in electrochemical and fluorescence experiments.

Fluorescence Measurements of DNA Switching. DNA switching experiments were performed in a thin-layer electrochemical cell provided by Prof. Bruce Gale of the University of Utah (Figure S2). The cell consists of a 3 in. × 1 in. glass slide upon which two pairs of Pt lines were deposited. The cell itself was formed from two polydimethylsilane (PDMS) layers contacted to the glass slide. The first layer was a 100-μm thick double-sided PDMS tape in which two 30 mm long × 1 mm wide fluidic channels were cut. The second PDMS layer, also of 100 μm thickness, was laid on top of the first to complete the channels. A circular chamber 4 mm in diameter was cut into the PDMS layers in the middle of each fluidic channel to form the cell. Two holes 1 mm in diameter were punched at the ends of each channel and connected to Teflon inlet and outlet tubes. One of the Pt electrodes was directly used as the counterelectrode. The exposed end of the other was coated with Ag paste and used as an Ag quasi-reference electrode. During both electrochemical and fluorescence experiments, the GCE, which served as the working electrode, was

pressed on top of the open PDMS chamber to complete the electrochemical cell. The cell was filled by pumping buffer solution through the fluidic channels using a syringe pump.

During DNA switching experiments, the open circuit potential (OCP) of the GCE was measured first. The OCP reflects the electrode potential in the equilibrated state. It was found to vary from −0.09 to 0.11 V vs the Ag quasi-reference electrode, depending on buffer concentration and ds-DNA length (see Table S1). A square waveform with potentials alternating between ±200 mV (vs OCP) was applied to the GCE with a potentiostat (CH Instruments) to drive ds-DNA reorientation. Current and potential profiles were recorded with 5 ms time resolution.

Fluorescence measurements of ds-DNA reorientation were made on one of two inverted fluorescence microscopes (Nikon, see Figure S3), both of which have been described previously.[15,16] FAM6 fluorescence was excited using 488 nm light from a solid-state laser. The excitation light (500 μW) was first reflected from a dichroic beamsplitter (Chroma, 505DCLP) and was then focused into the back aperture of either a 50×, 0.55 NA objective (Nikon, CF Plan) or a 100× 0.8 NA objective (Nikon, CF Plan), producing illuminated areas of ∼50 μm^2 and ∼25 μm^2 on the GCE, respectively. FAM6 fluorescence was collected with the same objective, and subsequently passed back through the dichroic beamsplitter and a bandpass filter (Chroma, HQ535/50M). It was then imaged onto a thermoelectrically cooled electron multiplying CCD camera (Andor, iXon DU-897). Fluorescence images were recorded at frame rates of 8 frames/s and 18 frames/s, depending on the specific pixel binning conditions (1 × 1 or 16 × 16) employed. Different electron multiplying (EM) gains (from 8 to 300) were also explored to achieve suitable signal-to-noise ratios. To allow for comparison of data recorded under different conditions, data acquired at higher frame rates were down-sampled to match the time resolution of data recorded at lower frame rates. The signal levels were also appropriately corrected for differences in integration times, pixel binning, and EM gain levels.

Electrochemical Characterization. Further electrochemical measurements were carried out in a larger Teflon cell. An O-ring of 3.0 mm inside diameter was used to seal the GCE against the Teflon cell so that only an area of 0.071 cm^2 on the GCE was exposed to 0.2−0.5 mL of solution. An Ag/AgCl (4 M KCl) reference electrode and a Pt coil counterelectrode were used in a three-electrode setup. The electrolyte solution was purged with nitrogen for 5 min prior to use to remove oxygen. The EDL capacitance was determined by cyclic voltammetry (CV) in 10 mM Tris-HCl buffer at a scan rate of 100 mV/s. The DNA density was quantified by chronocoulometry (CC), following a method reported by Steel, et al.[17] In this method, DNA density is determined by measuring the amount of $Ru(NH_3)_6^{3+}$ (Sigma-Aldrich) that is required to fully compensate the negative charges of the ds-DNA.[17] For these experiments, the GCE was first incubated in 50 μM $Ru(NH_3)_6^{3+}$ in 10 mM Tris-HCl buffer. Under these conditions, the $Ru(NH_3)_6^{3+}$ is strongly adsorbed to the DNA, with each $Ru(NH_3)_6^{3+}$ compensating the charge of three phosphate groups. The charge passed during the reduction of $Ru(NH_3)_6^{3+}$ to $Ru(NH_3)_6^{2+}$ was then measured over a period of 4 s after the electropotential was switched from +0.2 V to −0.3 V. The results were compared to those obtained in blank 10 mM Tris-HCl buffer to determine the amount of adsorbed $Ru(NH_3)_6^{3+}$ and, hence, the surface coverage of ds-DNA.

RESULTS

Density of ds-DNA on Modified GCEs. The density of DNA immobilized on the electrode surface was determined by chronocoulometry, as described in the Experimental Section. Figure S4 plots the measured charge, Q, passed as a function of $t^{1/2}$ during the reduction of adsorbed $Ru(NH_3)_6^{3+}$. The intercept obtained by extrapolating the linear portion of the curve to $t^{1/2} = 0$ (see Figure S4) represents the sum of the EDL charge accompanying the associated potential step, Q_{dl}, and the charge required to reduce the adsorbed $Ru(NH_3)_6^{3+}$, Q_{ads}. The value for Q_{dl} was independently determined from identical measurements performed in blank 10 mM Tris-HCl buffer. The complete results of these experiments are given in Table S2, which shows that Q_{ads} = 0.4692 μC. This value was then used to find the surface density of ds-DNA by:[17]

$$\Gamma_{DNA} = \Gamma_0\left(\frac{Z}{m}\right)N_A = \frac{Q_{ads}}{nFA} \times \frac{Z}{m} \times N_A \quad (1)$$

Here n = 1 is the number of electrons involved in the redox reaction per molecule, Z = 3 represents the number of nucleotides compensated by each $Ru(NH_3)_6^{3+}$, and m is the total number of nucleotides (m = 68 for 34-mer ds-DNA). As listed in Table S2, the average density of the 34-mer ds-DNA was determined to be 1.8 × 10^{12}/cm^2, giving an average surface area per ds-DNA molecule of 55 nm^2. This corresponds to an average spacing for the surface-bound ds-DNA molecules of ∼8.0 nm (assuming a hexagonal lattice), which is smaller than the length of 34-mer ds-DNA (11.22 nm).

Reorientation Dynamics of ds-DNA on GCEs. Figure 1a shows a representative potential waveform applied to the GCE to induce DNA reorientation. In most experiments, the electropotential was stepped between ±200 mV (all potentials are given vs OCP) at 2.00 s intervals. Figure 1b shows the background-corrected fluorescence profile obtained from FAM6-labeled 34-mer ds-DNA at a hexylamine-passivated GCE in 0.02× PBS. These data show that FAM6 fluorescence is modulated in registry with the potential waveform. Consistent

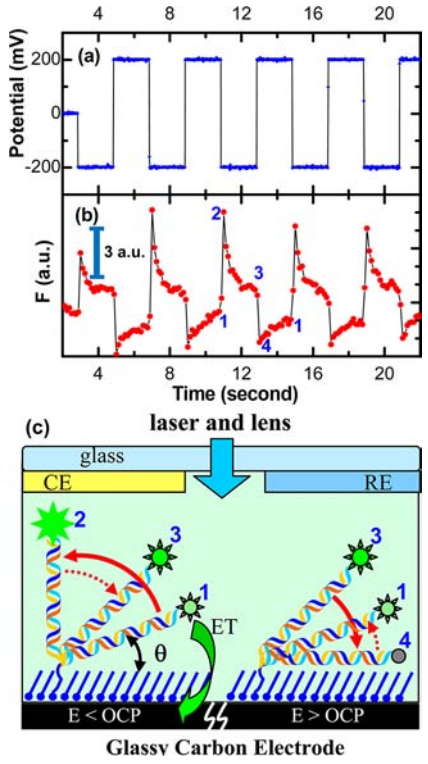

Figure 1. (a) Representative potential waveform applied to the GCE. (b) Background-corrected fluorescence intensity profile obtained from FAM6-labeled 34-mer ds-DNA attached to a hexylamine-passivated GCE while the potential was stepped between ±200 mV vs OCP in 0.02× PBS. (c) Optical/electrochemical cell used in the ds-DNA reorientation studies, including a simple model for ds-DNA orientation and FAM6 fluorescence at the positions labeled in (b). CE and RE represent the counterelectrode and reference electrode, respectively.

dx.doi.org/10.1021/ja304512k | J. Am. Chem. Soc. 2012, 134, 14467−14475

with previous observations by Rant, et al.,[6−8] the fluorescence abruptly increased when the potential was stepped to −200 mV and immediately dropped upon switching to +200 mV. The initial response in each case was much faster than the 55 ms temporal resolution available at the highest frame rates employed (Figure 1b was recorded at 8 frames/s). However, the fluorescence signal obtained did not remain at constant levels after potential switching, but rather exhibited additional dynamics that have not previously been reported. Specifically, after the initial abrupt increase or decrease in signal, slow relaxation of FAM6 fluorescence to intermediate values was observed. In this case, the slower dynamics occurred on a time scale of ∼0.35 s upon switching to −200 mV (see Figure 1b). These additional slow dynamics were observed in numerous replicate studies performed on several different GCEs. They are attributed to slow orientational relaxation of the ds-DNA from a transient orientation state that appears immediately after the potential step.

Careful control experiments demonstrated that the slow dynamics were not caused by the CCD camera or other optical, electronic, or electrochemical artifacts. Camera and optical artifacts were ruled out by collecting the fluorescence from polystyrene beads supported on a glass slide, while switching the laser source on and off using a fast electronic shutter (data not shown). All signal dynamics associated with laser modulation in these experiments were faster than the instrument time resolution (55 ms). As shown in Figure S5a (SI) chronoamperometry (CA) data acquired using the same cell and electropotential waveform showed a fast exponential decay with a time constant of 0.011 s. This value represents the RC time constant of the cell and demonstrates that the slow fluorescence dynamics observed (Figure S5b) were not limited by the electrochemical cell.

The slow relaxation observed in the FAM6 fluorescence could be due to effects other than ds-DNA reorientation. For example, when present at sufficient concentrations, dissolved oxygen is known to quench the fluorescence of fluorescein dyes.[18] Diffusion-limited faradaic generation and/or reduction of dissolved oxygen could therefore also be a source of the slow modulation in FAM6 fluorescence. However, detailed calculations show that, at the oxygen levels present (equilibrated with the atmosphere), modulation of FAM6 fluorescence would be at most 0.4% of the observed signal, were it being electrochemically removed and regenerated. The amplitude of fluorescence modulation is at least an order of magnitude larger, even in experiments showing weak modulation. Likewise, FAM6 fluorescence is also expected to be pH-dependent.[19] Electrochemical generation of H^+ and OH^- at the GCE and counterelectrode surfaces is a more important factor that could also contribute to the slow FAM6 fluorescence dynamics. Such pH-dependent effects cannot be altogether neglected. Estimates of the possible change in pH at the electrode surface (i.e., within one diffusion layer) following a potential step indicate such effects could be the dominant source of signal modulation at low buffer concentrations (0.0067× PBS). At the highest buffer concentration (0.2× PBS), the relatively small changes in pH that could occur should yield at most a few percent modulation (i.e., <10%) in the signal. As a whole, these calculations show that, were changes in pH the dominant source of the slow signal relaxation, dramatic FAM6 fluorescence modulation would be observed following a positive potential step at low buffer concentrations with much smaller modulation occurring at high concentrations and for negative potential steps. As shown below, the observed trend with buffer concentration is different and much weaker than expected from changes in pH. Finally, no signal modulation was observed when the PBS electrolyte was replaced by a zwitterionic buffer (see Figure S6, SI). It is therefore concluded that orientational relaxation of the ds-DNA and associated distance-dependent quenching of FAM6 fluorescence to the GCE surface are likely the primary cause of the observed slow dynamics.

It should also be noted that the OCP was used as the reference potential in these studies, rather than the potential of zero charge (PZC). The charge on the electrode surface is governed primarily by the negatively charged, surface-bound ds-DNA, at the OCP. The OCP corresponds most closely to the equilibrated surface structure (including the orientation state of the DNA) in the absence of external potential bias and was therefore deemed to be the most appropriate reference potential for these experiments. The OCP was measured prior to the start of every experiment (see Table S1, SI), and the applied potentials were set to ±200 mV of its value.

The dynamic DNA movements associated with the potential-dependent changes in FAM6 fluorescence (Figure 1b) can be described by a simple model of end-tethered rigid rods, as shown in Figure 1c. The assumption that the ds-DNA behaves as rigid rods is supported by its ∼50 nm persistence length.[20] As the electropotential was switched, the electrostatic force generated a torque on the negatively charged ds-DNA, causing the tilt angle θ to vary. The magnitude of the torque depends on the strength of the electric field within the EDL, which decreases rapidly with distance from the electrode surface. It also depends upon the charge density along the ds-DNA and on the ionic composition of the EDL.

Figure 1c illustrates four representative orientations of the ds-DNA molecules that are meant to qualitatively depict the ds-DNA orientation state at each of the labeled points on the fluorescence profile shown in Figure 1b. Position 1 corresponds to the orientationally relaxed state that occurs several seconds after switching the electropotential to +200 mV. At this point (10.76 s in Figure 1b), the ds-DNA molecule is tilted slightly away from the electrode surface and FAM6 fluorescence is observed to be relatively low due to quenching by the GCE (see below).

Upon switching of the electropotential to −200 mV (10.87 s in Figure 1b), the ds-DNA experiences a strong repulsive force that causes its abrupt reorientation from position 1 to position 2. FAM6 fluorescence reaches a maximum at position 2. At this point the ds-DNA is assumed to be oriented approximately perpendicular to the GCE surface, with the FAM6 label at its greatest distance from the electrode. Fast reorientation of the ds-DNA following the potential step is accompanied by rapid flux of cations toward the GCE surface, as the charges in the EDL rearrange. Establishment of the new EDL includes a time-dependent thinning of the EDL and associated variations in the electrostatic torque on the ds-DNA molecules. These primary EDL dynamics all occur within the first frame recorded by the camera after a potential step, as indicated by the 0.011 s decay time in the CA data (see Figure S5), and are not observed in the fluorescence traces. Slow relaxation of the ds-DNA orientation state toward position 3 then begins to occur. In this process, the ds-DNA tilts back toward the electrode surface, as evidenced by the slow decrease in FAM6 fluorescence over the subsequent ∼2 s period. During this period, the repulsive electrostatic force on the ds-DNA

molecules is reduced since a shorter segment of the ds-DNA resides in the thinned EDL. The ds-DNA molecules gradually reach an equilibrium orientation which is determined by the repulsive force and thermal Brownian motion.[21,22] In the next potential step (12.87 s in Figure 1b), the electropotential was switched back to +200 mV. Accordingly, the electrostatic force on the ds-DNA switched from repulsion to attraction, and the ds-DNA molecules quickly reorient to align approximately parallel to the GCE surface, designated as position 4. FAM6 fluorescence drops abruptly to its minimum value at this point as the dye makes its closest approach to the electrode. Movement of the negatively charged DNA molecules is again accompanied by fast, primary reconstruction of the EDL on a time scale that is too fast to observe in these experiments. These dynamics are again followed by the slow relaxation of the ds-DNA orientation over the course of ~2 s from position 4 back to position 1, an orientation similar to the starting position of the potential cycle. As the ds-DNA relaxes, FAM6 fluorescence is observed to gradually increase. Interestingly, the tilt angle at position 3 is larger than that at position 1, since the ds-DNA at the former position was subjected to a repulsive force, whereas at the latter, it experiences an attractive electrostatic force, both of which equilibrated with thermal ds-DNA motions.

Effects of Buffer Concentration and DNA length. The potential-dependent switching of ds-DNA is governed by the spatial overlap of the ds-DNA with the strong fields of the EDL. Due to screening effects, the electropotential decays with distance (x) from the electrode surface as $\exp(-x/\lambda_D)$. The characteristic decay distance, λ_D, is known as the Debye length, and its value is strongly dependent on the buffer concentration. In 1× PBS buffer, λ_D = 0.7 nm,[23] whereas its value increases to 4.9 nm for the 0.02× PBS solution used in Figure 1. Therefore, the dynamics of DNA reorientation are also expected to vary with buffer concentration. Figure 2 shows the results obtained for studies of 34-mer ds-DNA in 0.0067×, 0.02×, 0.067×, and 0.2× PBS. These data all show profiles similar to that of Figure 1b, demonstrating the reproducibility and generality of the reorientation dynamics described above. Similar ds-DNA switching behavior was also observed from longer 45-mer ds-DNA, as shown in Figure 3, which plots representative results

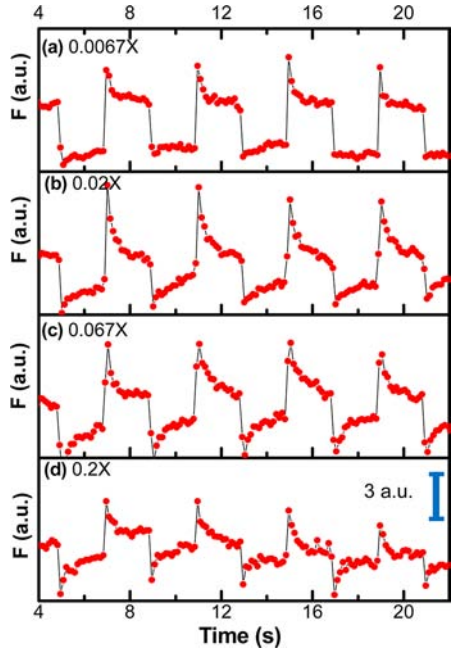

Figure 2. (a–d) Fluorescence profiles obtained from FAM6-labeled 34-mer ds-DNA in various diluted PBS buffers, as the electrode potential was switched between ±200 mV vs OCP.

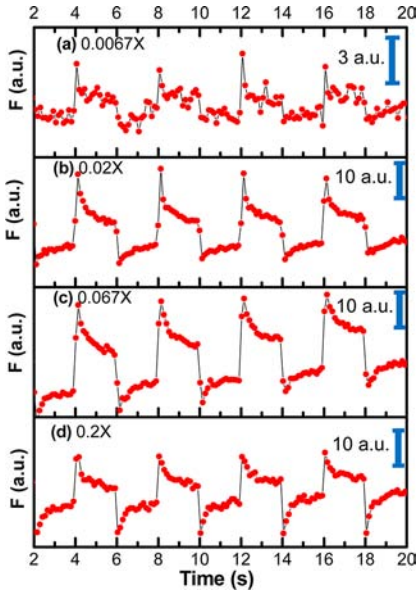

Figure 3. (a–d) Fluorescence profiles obtained from FAM6-labeled 45-mer ds-DNA in various diluted PBS buffers, as the electrode potential was switched between ±200 mV vs OCP.

obtained in the same four diluted PBS buffer solutions. The magnitude of the fluorescence modulation for the 45-mer ds-DNA is generally larger than for 34-mer ds-DNA, as would be expected for distance-dependent FAM6 quenching to the electrode surface.

The amplitudes of the switching dynamics depicted in Figures 2,3 exhibit a clear dependence on buffer concentration. The difference between the fluorescence maximum and minimum (i.e., $F_2 - F_4$) in each potential cycle reflects the difference in FAM6 distance (i.e., $d_2 - d_4$) from the GCE surface for these positions. The data shown in Figures 2,3 depict an initial increase in amplitude with increasing buffer concentration. The maximum amplitude is observed at 0.067× PBS for both 34-mer and 45-mer ds-DNA. A further increase in buffer concentration to 0.2× PBS leads to a subsequent decrease in amplitude with no fluorescence modulation observed above the background noise in 1× PBS. As noted above, the Debye length is only 0.7 nm in 1× PBS, and hence, the electropotential has little effect on the ds-DNA orientation in concentrated buffer. Similar results were obtained when a zwitterionic buffer was employed as the supporting electrolyte (see SI, Figure S6). The Debye length in this case is much longer, greatly reducing the EDL field strength and the modulation of ds-DNA orientation. This behavior clearly demonstrates that the dynamics observed arise from effects occurring within the EDL at the GCE surface.

Time Scales of the Slow ds-DNA Relaxation Dynamics. The relatively slow relaxation of FAM6 fluorescence observed between positions 2 and 3, and positions 4 and 1 (Figure 1) could be nicely fit to a single exponential function, including a constant offset, in each case. Parts a and b of Figure 4 show representative fluorescence profiles for 34-mer and 45-mer ds-

dx.doi.org/10.1021/ja304512k | J. Am. Chem. Soc. 2012, 134, 14467–14475

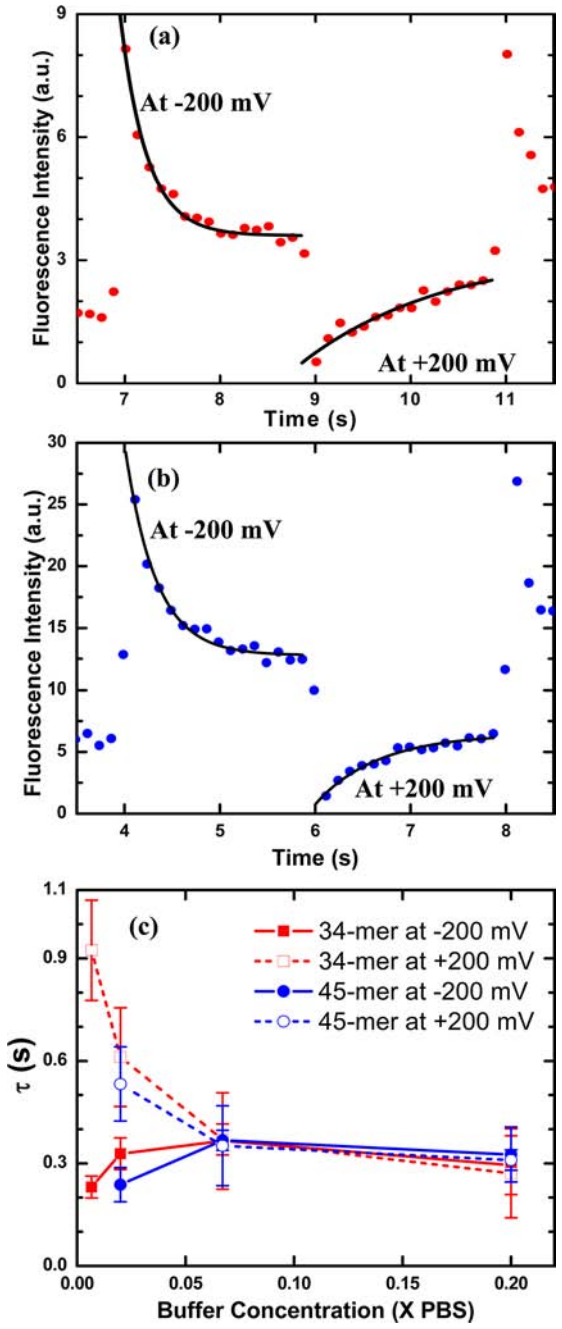

Figure 4. Dynamic fluorescence profiles obtained during electrical switching of (a) 34-mer and (b) 45-mer ds-DNA on a GCE in 0.02× PBS. Each profile has been fitted to an exponential function. (c) Time constants obtained from exponential fits to fluorescence profiles recorded at negative and positive potentials, plotted as a function of PBS buffer concentration.

DNA in 0.02× PBS and their associated fits, respectively. The starting point of each fit was fixed to the time that the electropotential was switched. The fitted values of the decay amplitude and the offset were used in the quantitative analysis of FAM6 fluorescence, as discussed below.

The fits also provide important information on the time scale of signal relaxation. From these data, it is clear that the relaxation time following a potential step to −200 mV (0.28 s) is shorter than that following a step to +200 mV (0.77 s), for 34-mer ds-DNA in 0.02× PBS. Similar results are obtained from 45-mer ds-DNA under the same conditions (0.32 and 0.66 s, respectively). Figure 4c plots the relaxation time vs buffer concentration for both ds-DNA lengths. These two data sets show similar trends; the relaxation time after switching of the potential to +200 mV (τ_+) in each became dramatically shorter as the buffer concentration was increased from 0.0067× PBS. In contrast, the relaxation time following a change to −200 mV (τ_-) exhibited an opposite trend, becoming somewhat longer at higher PBS concentrations.

Quantitative Model for Dipole−Electrode Energy Transfer. The variation in FAM6 fluorescence accompanying ds-DNA reorientation can be attributed to fluorescence quenching due to dipole−electrode energy transfer.[7,13,24] In this case, the rate of energy transfer, k_{et}, decreases either as d^{-3} or as d^{-4}, where d is the dye−surface distance.[12] The relative importance of these two models depends on distance and on whether quenching occurs to the bulk or surface of the electrode, respectively.[7,12,13,24] We adopt the d^{-4} dependence, as previously reported in the literature,[13,25] with

$$k_{et} = \frac{1}{\tau}\left(\frac{d_o}{d}\right)^4 \tag{2}$$

Here, τ is the fluorescence lifetime of the dye in the absence of energy transfer and d_o is the characteristic quenching distance at which $k_{et} = 1/\tau$. Energy transfer competes with radiative emission and other nonradiative processes to deactivate photoexcited FAM6, with the quantum yield for energy transfer, ϕ_{et}, given by

$$\phi_{et} = \frac{k_{et}}{k_r + k_{nr} + k_{et}} \tag{3}$$

Combining eqs 2 and 3, and using $1/\tau = k_r + k_{nr}$, it is easily shown that

$$\phi_{et} = \frac{1}{1 + (d/d_o)^4} \tag{4}$$

The ratio of the fluorescence intensity at finite distance d to that at infinite distance from the electrode surface can then be expressed as

$$\frac{F_d}{F_\infty} = 1 - \phi_{et} = \frac{1}{1 + (d_o/d)^4} \tag{5}$$

The value of d_0 can be calculated using an equation adopted from Jennings, et al.:[13]

$$d_0 = \left(0.225\frac{c^3\phi_{dye}}{\omega_{dye}^2\omega_F k_F}\right)^{1/4} \tag{6}$$

where c is the speed of light in a vacuum, ϕ_{dye} the fluorescence quantum yield of the dye (0.8 for FAM6), ω_{dye} the angular frequency of its electronic absorption (3.65×10^{15} s^{-1}), ω_F the Fermi frequency of the electrode (6.99×10^{15} s^{-1} for the GCE, derived from its work function, assumed to be 4.6 eV), and k_F is the Fermi wave vector for the GCE (1.10×10^8 cm^{-1}). The calculated value, d_0 = 8.30 nm, is slightly larger than reported for a similar dye on Au nanoparticles (d_0 = 7.63 nm).[13]

It should be noted that the DNA employed incorporates a dimethylaminoazobenzene (Dabcyl) quencher at the end closest to the GCE surface. While its presence complicates the analysis, the contributions of Dabcyl quenching are believed to be relatively unimportant. Fluorescence quenching in this

dx.doi.org/10.1021/ja304512k | J. Am. Chem. Soc. 2012, 134, 14467−14475

case occurs by Förster energy transfer, which exhibits a much shorter d^{-6} distance dependence. The characteristic distance (d_o for Förster energy transfer) for FAM6 quenching to Dabcyl is also smaller (~4.8 nm). The rate of Förster energy transfer is therefore estimated to be <20% of the rate of quenching to the electrode surface at position 1 (Figure 1c, see below for estimates of the FAM6−electrode distance) and is even less significant at positions 2 and 3.

Figure 5a shows the simulated curve for F_d/F_∞ vs d using eq 5, with d_0 = 8.30 nm. On the basis of this model, the dye−surface distance d at each characteristic position illustrated in Figure 1c can be estimated from the fluorescence profiles obtained during electropotential switching. Two important assumptions are employed in making these determinations: (1) The fluorescence at position 4 is assumed to be almost completely quenched (i.e., $F_4 \approx 0$ at the minimum of each fluorescence profile), with the ds-DNA lying flat on the GCE surface. The minimum dye−surface distance in this case is taken to be d_4 = 0.76 nm, as defined by the thickness of a hexylamine monolayer incorporating fully extended, all-*trans*-methylene chains.[26] (2) At position 2, for 0.067× PBS (i.e., the data exhibiting maximum amplitude), the ds-DNA is assumed to be oriented perpendicular to the surface, with both the aminoC7 linker and the ds-DNA fully extended. The dye−surface distance at this point (d_2) thus includes the full lengths of ds-DNA, the dT (used for attaching Dabcyl at the thymine), and the aminoC7 linker. It is estimated to be 12.43 nm for 34-mer and 16.06 nm for 45-mer ds-DNA, respectively. However, it must be stressed that the exact FAM6−GCE distance is strictly unknown. As a final caveat, it should be noted that the ds-DNA molecules do not take on a single, fixed orientation. Rather, they exhibit thermally driven diffusion through a range of angles around the field-aligned state.[27,28] As a result, the distances (d) reported actually reflect weighted averages of the range of FAM6−GCE distances that occur at each potential.

With the above assumptions, a value for F_∞ was established for each ds-DNA length and was subsequently used to normalize all fluorescence signals. In the present experiments, F_∞ was determined to be 13.24 and 40.29 for 34-mer and 45-mer ds-DNA, respectively. F_∞ increases with ds-DNA length as generally expected, but quantitative comparisons could not be drawn between these data for a number of reasons, including sample-to-sample variability in the absolute fluorescence intensity obtained due to variability in the level of GCE functionalization, variations in the laser intensity (and focus) at the sample surface, and changes in the optical collection and detection system made to optimize signal-to-noise levels and time resolution. Nevertheless, the results were found to be highly reproducible for individual samples and for data acquired on the same day.

Application of eq 5 to the analysis of these data then allows for estimation of the average FAM6 distance, d, from the GCE surface, and hence the ds-DNA orientation state, at all points along the fluorescence profiles, F. The average distances at positions 1 and 3 (d_1 and d_3, respectively) are specifically highlighted, as shown in Figure 5a. The dye−surface distance at position 3 is estimated to be 7.64 and 8.60 nm for 34-mer and 45-mer ds-DNA, respectively. For position 1, values of 6.59 and 6.40 nm are obtained.

Equation 5 also affords the means to assess buffer concentration-dependent variations in FAM6 distance from the GCE surface. Data for position 2 are provided in panels b and c of Figure 5 that specifically plot F_2/F_∞ and d_2 vs PBS concentration, respectively. These data show that 0.067× PBS yields the maximum fluorescence modulation amplitude, whereas lower and higher PBS concentrations produce smaller amplitudes. It is concluded that FAM6 reaches its maximum

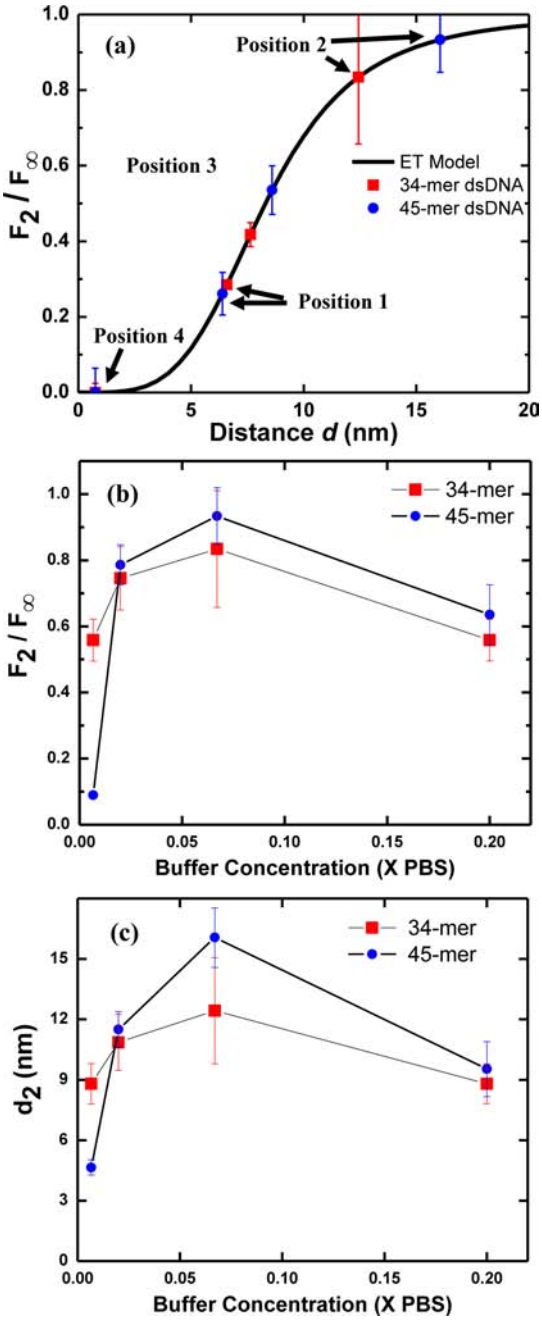

Figure 5. (a) Normalized fluorescence efficiency (F_d/F_∞) of 34-mer and 45-mer ds-DNA in 0.067× PBS buffer vs dye−surface distance due to quenching by energy transfer between the FAM6 dye and the electrode surface as described by eq 5. At this buffer concentration, the dye−surface distances d_2 and d_4 are assumed to be at the fully extended length of the ds-DNA molecule and 0.76 nm (the thickness of the hexylamine passivation layer), respectively. The dye−surface distances at other characteristic positions, such as 1 and 3, are derived by locating the measured fluorescence intensities on the energy transfer curve. (b) Dependence of the normalized fluorescence efficiency at position 2 (F_2/F_∞) on PBS buffer concentration. (c) Variation of the maximum dye−surface distance d_2 as a function of buffer concentration.

dx.doi.org/10.1021/ja304512k | J. Am. Chem. Soc. 2012, 134, 14467−14475

distance from the GCE surface immediately after a potential step to −200 mV in 0.067× PBS. In more dilute and more concentrated buffer, the ds-DNA is not reoriented to the same extent due to weaker interactions between the ds-DNA and the EDL field.

DISCUSSION

As has been described previously,[6−8] the data presented above are consistent with a change in the orientation state of electrode-bound ds-DNA as the electropotential at the GCE surface is altered. These changes can be monitored by recording the fluorescence from a dye label attached to the distal end of the DNA. In the present experiments, the initial reorientation dynamics were found to be very fast, as reported in the literature.[6−8] However, new orientational relaxation dynamics were also found to follow a change in the electropotential. These dynamics were manifested as a much slower (∼0.1−0.9 s) relaxation of the FAM6 fluorescence from the extremes exhibited immediately after potential switching to intermediate values. Both the amplitudes and time scales for these dynamics were shown to depend on the sign of the applied electropotential, the length of the ds-DNA, and the buffer concentration. No instrumental, electronic, or electrochemical artifacts could be identified to explain the occurrence of these dynamics. Rather, the above observations indicate that these new dynamics are directly linked to processes occurring in the EDL. Importantly, the dynamics are too slow to be explained by conventional EDL charging.

While the exact origins of the new dynamics are currently unknown, several possible explanations exist. One possibility may be steric interactions between the electrode-bound ds-DNA molecules. If the ds-DNA molecules are too closely spaced, they will interfere with each other as they fold onto or move away from the electrode surface. As described above, the DNA density on the GCE surface is 1.8×10^{12} cm^{-2}, a value just above that reported by Rant, et al. (8×10^{11} cm^{-2})[6−8] for the onset of steric interactions. It was stated in this earlier work that only low-density ds-DNA exhibited a fast response to a change in electropotential. While such interactions would lead to slower reorientation dynamics, it is believed they would cause a slowing of the initial response to a change in the potential, not the appearance of new dynamics occurring after fast reorientation of the ds-DNA. Studies of the dependence of these dynamics on ds-DNA density will be reported in the future.

Another possible explanation is that the negative charges in the electrode-bound ds-DNA layer significantly alter the establishment of the EDL. From the chronocoulometric results discussed earlier (parameters listed in Table S2) and accounting for Manning condensation of sodium ions along the phosphate−sugar backbone,[29] a 34-mer ds-DNA layer on the GCE would consist of a negative charge density of ∼5 μC/cm.^{2} If only these negative charges were attracted to the GCE surface when a +200 mV electropotential is applied, it would be enough to fully charge a double-layer capacitor of 25 μF/cm^2. This value is very close to the reported value of 24−36 μF/cm^2 for bare GCEs,[30] suggesting that the ds-DNA may comprise the entire negative charge of the EDL at +200 mV. Likewise, at −200 mV, many more positive ions are needed to move into the EDL than at the bare GCE so that the negative charge of surface-attached ds-DNA can be offset. As a result, after the fast initial DNA reorientation to push the negative charge away from the electrode surface, counterions would then migrate from the bulk solution to balance the excess charge on the DNA, causing the DNA molecules to relax. The movement of these counterions and the relaxation of the negatively charged ds-DNA would thus constitute additional dynamics beyond those that "normally" occur during EDL reconstruction following a change in potential. Future investigations will explore this possibility in more detail.

Finally, it is possible that the slow relaxation dynamics are a consequence of complex time-dependent interactions between the reorienting, electrode-bound ds-DNA and the time-dependent EDL field. As shown in panels b and c of Figure 5, "complete" reorientation of the ds-DNA requires optimum overlap between the EDL field and the ds-DNA molecules. If the buffer concentration is too large, the length of the DNA exposed to a strong field is too short to fully reorient the DNA. Likewise, if the buffer is too dilute, the field strength is insufficient to cause "complete" reorientation. Importantly, the EDL field and its spatial overlap with the reorienting ds-DNA both change in time during EDL reconstruction. Therefore, it may be that stronger interactions between the DNA and the EDL field occur at some point early on during EDL reconstruction than would be expected for the equilibrated EDL. As the EDL reaches equilibrium conditions, the energy barrier to ds-DNA reorientation by Brownian motion would be moderated, allowing for subsequent relaxation from the initial orientation state. For a small reduction in the energy barrier, the relaxation dynamics may be very slow. Conclusive evidence for this last model could be obtained from sophisticated Brownian dynamics simulations of the entire process, including EDL charging dynamics.[21,22]

CONCLUSIONS

The potential-dependent reorientation dynamics of ds-DNA molecules at planar glassy carbon electrode surfaces were investigated. Rapid (instrument-limited, i.e., subms) reorientation of the DNA perpendicular and parallel to the electrode surface was observed to follow a step in the electrode potential to negative and positive values, respectively. Such dynamics have been described previously for ds-DNA reorientation at gold electrode surfaces. However, much slower (i.e., ∼0.1−0.9 s) ds-DNA relaxation dynamics were also observed to follow the fast dynamics in the present studies. These dynamics have not previously been described in the literature. The amplitudes and time scales for these latter dynamics were found to depend on buffer concentration and length of ds-DNA employed. The results show that these dynamics depend upon the nature of the EDL at the GCE surface. Several possible explanations for the origins of the dynamics were proposed. Rigorous identification of their cause will require additional experimentation and sophisticated computer modeling. A better understanding of ds-DNA dynamics at electrode surfaces will lead to improved models for potential-dependent ds-DNA reorientation and will facilitate the development of advanced electrochemical devices for DNA detection.

ASSOCIATED CONTENT

Supporting Information

Additional experimental details and data sets. This material is available free of charge via the Internet at http://pubs.acs.org.

AUTHOR INFORMATION

Corresponding Author

higgins@ksu.edu (D.A.H.); junli@ksu.edu (J.L.)

Notes

The authors declare no competing financial interest.

■ ACKNOWLEDGMENTS

Kansas State University, Early Warning Inc., the Kansas Biosciences Authority, and the Department of Homeland Security are thanked for their support of this work. Some instrumentation employed in the fluorescence studies was provided by the Office of Basic Energy Sciences at the U.S. Department of Energy (DE-SC0002362).

■ REFERENCES

(1) Cosnier, S.; Mailley, P. *Analyst* **2008**, *133*, 984−991.
(2) Drummond, T. G.; Hill, M. G.; Barton, J. K. *Nat. Biotechnol.* **2003**, *21*, 1192−1199.
(3) Sosnowski, R. G.; Tu, E.; Butler, W. F.; O'Connell, J. P.; Heller, M. J. *Proc. Natl. Acad. Sci. U.S.A.* **1997**, *94*, 1119−1123.
(4) Heaton, R. J.; Peterson, A. W.; Georgiadis, R. M. *Proc. Natl. Acad. Sci. U.S.A.* **2001**, *98*, 3701−3704.
(5) Mahajan, S.; Richardson, J.; Brown, T.; Bartlett, P. N. *J. Am. Chem. Soc.* **2008**, *130*, 15589−15601.
(6) Rant, U.; Arinaga, K.; Fujita, S.; Yokoyama, N.; Abstreiter, G.; Tornow, M. *Nano Lett.* **2004**, *4*, 2441−2445.
(7) Rant, U.; Arinaga, K.; Scherer, S.; Pringsheim, E.; Fujita, S.; Yokoyama, N.; Tornow, M.; Abstreiter, G. *Proc. Natl. Acad. Sci. U.S.A.* **2007**, *104*, 17364−17369.
(8) Kaiser, W.; Rant, U. *J. Am. Chem. Soc.* **2010**, *132*, 7935−7945.
(9) Bard, A. J.; Faulkner, L. R. *Electrochemical Methods, Fundamentals and Applications*; John Wiley and Sons: New York, 1980.
(10) McCreery, R. L. *Chem. Rev.* **2008**, *108*, 2646−2687.
(11) Arumugam, P. U.; Chen, H.; Siddiqui, S.; Weinrich, J. A. P.; Jelelowo, A.; Li, J.; Meyyappan, M. *Biosens. Bioelectron.* **2009**, *24*, 2818−2824.
(12) Persson, B. N. J.; Lang, N. D. *Phys. Rev. B* **1982**, *26*, 5409−5415.
(13) Jennings, T. L.; Singh, M. P.; Strouse, G. F. *J. Am. Chem. Soc.* **2006**, *128*, 5462−5467.
(14) CalcTool: http://www.calctool.org/CALC/prof/bio/dna.
(15) Hou, Y.; Bardo, A. M.; Martinez, C.; Higgins, D. A. *J. Phys. Chem. B* **2000**, *104*, 212−219.
(16) Tran Ba, K. H.; Everett, T. A.; Ito, T.; Higgins, D. A. *Phys. Chem. Chem. Phys.* **2011**, *13*, 1827−1835.
(17) Steel, A. B.; Herne, T. M.; Tarlov, M. J. *Anal. Chem.* **1998**, *70*, 4670−4677.
(18) Arik, M.; Celebi, N.; Onganer, Y. *J. Photochem. Photobiol., A* **2005**, *170*, 105−111.
(19) Martin, M. M.; Lindqvist, L. *J. Lumin.* **1975**, *10*, 381−390.
(20) Bustamante, C.; Bryant, Z.; Smith, S. B. *Nature* **2003**, *421*, 423−427.
(21) Rant, U.; Arinaga, K.; Fujita, S.; Yokoyama, N.; Abstreiter, G.; Tornow, M. *Org. Biomol. Chem.* **2006**, *4*, 3448−3455.
(22) Sendner, C.; Kim, Y. W.; Rant, U.; Arinaga, K.; Tornow, M.; Netz, R. R. *Phys. Status Solidi A* **2006**, *203*, 3476−3491.
(23) Vacic, A.; Criscione, J. M.; Rajan, N. K.; Stern, E.; Fahmy, T. M.; Reed, M. A. *J. Am. Chem. Soc.* **2011**, *133*, 13886−13889.
(24) Alivisatos, A. P.; Waldeck, D. H.; Harris, C. B. *J. Chem. Phys.* **1985**, *82*, 541−547.
(25) Li, M.; Cushing, S. K.; Wang, Q.; Shi, X.; Hornak, L. A.; Hong, Z.; Wu, N. *J. Phys. Chem. Lett.* **2011**, *2*, 2125−2129.
(26) Lide, D. R., Ed. *CRC Handbook of Chemistry and Physics*, 85th ed.; CRC Press: New York, 2004.
(27) Anne, A.; Demaille, C. *J. Am. Chem. Soc.* **2006**, *128*, 542−557.
(28) Anne, A.; Demaille, C. *J. Am. Chem. Soc.* **2008**, *130*, 9812−9823.
(29) Manning, G. S. *Acc. Chem. Res.* **1979**, *12*, 443−449.
(30) Rice, R. J.; Pontikos, N. M.; McCreery, R. L. *J. Am. Chem. Soc.* **1990**, *112*, 4617−4622.